PROCEEDINGS OF
THE ROYAL SOCIETY B
BIOLOGICAL SCIENCES

Computer simulations show that Neanderthal facial morphology represents adaptation to cold and high energy demands, but not heavy biting

Journal:	*Proceedings B*
Manuscript ID	RSPB-2018-0085.R1
Article Type:	Research
Date Submitted by the Author:	11-Mar-2018
Complete List of Authors:	Wroe, Stephen; University of New England, Parr, William; University of New South Wales, School of Biological, Environmental and Earth Sciences Ledogar, Justin; University at Albany, Anthropology Bourke, Jason; University of New South Wales, Biological Earth and Environmental Science; Evans, Samuel; University of Newcastle, Mechanical Engineering Fiorenza, Luca; Monash University Benazzi, Stefano; Universita degli Studi di Bologna, Department of Cultural Heritage Hublin, Jean-Jacques; Max Planck Institute for Evolutionary Anthropology, Department of Human Evolution Stringer, Chris; Natural History Museum London, Kullmer, Ottmar; Senckenberg Research Institute, Department of Paleoanthropology and Messel Research Curry, Michael; University of New England Rae, Todd; Roehampton University, School of Health and Life Sciences Yokley, Todd; Metropolitan State University of Denver
Subject:	Evolution < BIOLOGY, Biomechanics < BIOLOGY
Keywords:	Neanderthal, Homo heidelbergensis, Computational Fluid Dynamics, Finite Element Analysis
Proceedings B category:	Palaeobiology

Computer simulations show that Neanderthal facial morphology represents adaptation to cold and high energy demands, but not heavy biting

Stephen Wroe[1,*], William C. H. Parr[2,*], Justin A. Ledogar[1], Jason Bourke[3], Samuel P. Evans[4], Luca Fiorenza[5], Stefano Benazzi[6,7], Jean-Jacques Hublin[7], Chris Stringer[8], Ottmar Kullmer[9], Michael Curry[1], Todd C. Rae[10], & Todd R. Yokley[11]

[1]Function, Evolution & Anatomy Research Lab, School of Environmental & Rural Science, University of New England, NSW, 2351,

[2]Surgical and Orthopaedic Research Laboratory (SORL),Level 1, Clinical Sciences Bld, Gate 6, Prince of Wales Clinical School, University of New South Wales (UNSW), Avoca St, Randwick, Sydney, NSW 2031, Australia

[3]Department of Biological Sciences, North Carolina State University, Athens, Ohio, USA

[4]School of Engineering, University of Newcastle, Callaghan, NSW, 2308, Australia

[5]Department of Anatomy and Developmental Biology, Monash University, Clayton, Victoria, 3800, Australia

[6]Department of Cultural Heritage, University of Bologna, Via degli Ariani 1, Ravenna, 48121, Italy

[7]Department of Human Evolution, Max Planck Institute for Evolutionary Anthropology, 04103 Leipzig, Germany

[8]Department of Earth Sciences, Natural History Museum, London SW7 5BD, UK

[9]Senckenberg Forschungsinstitut Frankfurt am Main, Abteilung Paläoanthropologie und Messelforschung, Sektion Tertiäre Säugetiere, Senckenberganlage 25, 60325 Frankfurt am Main, Germany

[10]Centre for Research in Evolutionary and Environmental Anthropology, University of Roehampton, London, UK

[11]Metropolitan State University of Denver, P.O. Box 173362, Campus Box 28, Denver, CO 80217-3362, USA

*These authors contributed equally to this work.

Three adaptive hypotheses have been forwarded to explain the distinctive Neanderthal face: 1) an improved ability to accommodate high anterior bite forces, 2) more effective conditioning of cold and/or dry air, and, 3) adaptation to facilitate greater ventilatory demands. We test these hypotheses using three-dimensional models of Neanderthals, modern humans, and a close outgroup (*H. heidelbergensis*), applying finite element analysis (FEA) and computational fluid dynamics (CFD). This is the most comprehensive application of either approach applied to date and the first to include both. FEA reveals few differences between *H. heidelbergensis*, modern humans and Neanderthals in their capacities to sustain high anterior tooth loadings. CFD shows that the nasal cavities of Neanderthals and especially modern humans condition air more efficiently than does that of *H. heidelbergensis*, suggesting that both evolved to better withstand cold and/or dry climates than less derived *Homo*. We further find that Neanderthals could move considerably more air through the nasal pathway than could *H. heidelbergensis* or modern humans, consistent with the propositions that, relative to our outgroup *Homo*, Neanderthal facial morphology evolved to reflect improved

capacities to better condition cold, dry air, and, to move greater air volumes in response to higher energetic requirements.

1. Introduction

Neanderthals (*Homo neanderthalensis*) are an "archaic" human species which persisted through multiple glacial-interglacial cycles in mid-late Pleistocene Eurasia. A number of craniofacial features distinguish Neanderthals from modern humans, including a wide, tall nasal aperture, a depressed nasal floor, a wide projecting nasal bridge, a retro-molar gap, "swept back" zygomatic arches and a depressed nasal floor [1, 2]. Whether, or to what degree, some of these features may represent adaptations to heavy para-masticatory activity (teeth as tools), better conditioning of cold, dry air, increased ventilatory flows in response to higher energetic demands, genetic drift, or simply retained plesiomorphies shared with earlier *Homo* has been the subject of longstanding debate [3-5], but the Neanderthal cranium is certainly distinctive [6].

Of the three adaptive hypotheses offering explanations for Neanderthal craniofacial evolution, the anterior dental loading hypothesis (ADLH), suggesting that that the Neanderthal face incorporates adaptations to sustain high loads applied to the incisors and/or canines, is perhaps the oldest. It has been underpinned by evidence of heavy wear on the anterior teeth in Neanderthals, although comparable wear may exist among contemporaneous modern humans [7]. Early arguments for the ADLH theorised that the Neanderthal face was better able to oppose rotation under loading on the anterior teeth around either transverse [4] or sagittal [8] axes. A more nuanced interpretation has been that facial prognathism in Neanderthals represents a trade-off between demands for high bite force at the anterior teeth and increasing the functional surface area of the molars for the mastication of resistant foods, while maintaining compressive forces at the temporomandibular joints during both anterior and postcanine loading [9]. Other studies have rejected the ADLH outright [10].

Similarly, the argument that the Neanderthal face incorporates adaptation to life in cold climates through an improved capacity to condition cold, dry, inspired air also remains controversial. The proposition that their large nasal cavities would have served to warm and humidify cold air more effectively [5] has been difficult to test quantitatively [11, 12]. The hypothesis that their well-developed paranasal sinuses [13] are a cold-adaptation has also been questioned. Some have asserted that Neanderthal paranasal sinuses are not particularly large [14], others have argued that paranasal size is largely irrelevant in the conditioning of inspired air [15]. Recent studies based on modern human samples have concluded that it is the shape, not the size of the nasal cavity, that primarily determines the capacity to warm and humidify inspired air [16]. It has been proposed that airway size likely relates to the energetics of the organism, whereas airway shape might be more indicative of physiology and climate [17].

A third hypothesis that might in part explain Neanderthal facial morphology is that it represents adaptation to facilitate greater ventilatory demands driven by high energy expenditures [18, 19]. High respiratory demands have been proposed for Neanderthals and other 'archaic' humans, such as *H. heidelbergensis*, based on evidence for relatively high body masses and routinely strenuous hunting/foraging behaviours [20]. Regarding Neanderthals, selective pressure may have been further increased by high cold resistance costs [21] as well as energetic hunting strategies [22].

Although considerable effort has been expended on addressing these explanations for Neanderthal facial morphology no extensive quantification of facial stressor strain regimes during biting have been performed. Regarding the modelling of heat transfer and humidification, CFD has previously been applied in vertebrate palaeontology and to some extant hominids [23, 24]. Most recently two modern humans have been compared to a partial model of a Neanderthal nasal passage [25]. Results showed that the partial Neanderthal was less efficient at conditioning cold, dry air than a modern north-eastern Asian, but slightly more efficient than a southern European. However, unlike the present study, this previous study only incorporated differences in external nasal aperture and the Neanderthal's internal nasal passage was not reconstructed. Moreover, no previous CFD analyses have included modelling of a close outgroup to modern humans and Neanderthals, or compared respiratory flow rates, meaning that CFD results have yet to be placed in a broader evolutionary context.

The application of quantitative 2D beam theory to craniofacial biomechanics represents a major advance over qualitative general comparisons, but 3D computer-based approaches, such as FEA, allow the biomechanics of whole structures to be analysed and compared based on a range of performance metrics [26-28]. In recent years FEA has been increasingly applied in palaeoanthropology [26, 29-32], boosted by improvements in virtual reconstruction methodologies (figure 1) and integration with geometric morphometrics (GMM) [33-35]. Importantly, FEA also allows the researcher to directly predict mechanical performance in great detail and compare it in comparative contexts [26]. Similarly, while CFD is a time-consuming process which limits sample sizes, it is the only means available that allows researchers to directly test the effects of geometry on fluid and heat flow in living and extinct taxa, whereas morphometric-based approaches are restricted to identifying correlations between morphology and variables such as diet or climate [24].

2. Material and methods

Materials. Models are based on computed tomography of the following specimens: Broken Hill 1, Mauer 1 (*Homo heidelbergensis*); La Ferrassie 1, La Chapelle-aux-Saints 1, Gibraltar 1, Le Moustier 1, Regourdou 1 (*H. neanderthalensis*); Mladeč 1 (Pleistocene *Homo sapiens*); NMB 1271 Khoe-San female, ULAC210 European male; AMNH 99/7889 Asian female, PM 0003 Asian male, AMNH 19.33 European female, AMNH 99.1/511 Inuit male, PM 1702, Inuit female, DO.P.004 European male, PM 1532 Pacific male, PM 0084 Peruvian female, UNC002 European male, and UNC013 African American male (recent *Homo sapiens*).

These latter two modern human specimens (CFD analyses only) were chosen because they represented a more polar-adapted (European) and more tropical (African) adapted nasal morphologies [16, 36].

Broken Hill 1 was selected as our outgroup because it is the most complete specimen commonly assigned to *H. heidelbergensis* [37]. Our selection of Neanderthal material was based on completeness. Remaining modern human specimens reflected the widest ethnographic range available.

Virtual reconstructions.

Fossil specimens were variably damaged or fragmentary. Where morphology was missing or damaged on one side of a specimen, but complete on the other, virtual reconstruction (step 1) was relatively straightforward [38] (Electronic Supplementary Material (~~figure 3,~~ ESM) figure S1), i.e., for Broken Hill 1 and Mladeč 1. In all three Neanderthals at least some bone, including internal portions of the nasal cavities are damaged or missing altogether. For these, a second step, 'warping', was applied after step 1 reconstruction, following established protocols [33, 39] (figure 1 & figures S2-S4 in ~~Electronic Supplementary Material (~~ESM~~)~~). The source mesh for warping was a recent modern *Homo sapiens* chosen for its particularly regular and symmetrical internal nasal morphology (ULAC-210).

Finite element analyses.

Model generation. For our FEA, 3D volume meshes were generated and loads applied on the basis of computed tomography, largely using previously described protocols [26, 29, 40, 41]. Segmentation was conducted in Mimics v17 (Materialise) and Finite element models (FEMs) were generated in 3-matic v8 (Materialise) based on a previously described approach [26, 41]. FEMs were kept at ~2 million tet4 elements and assigned a homogeneous property set [40]. Results can be influenced by differences in the distribution of materials [31, 42] and proportions of cortical and cancellous bone may vary across large size ranges [43]. However, size differences are not great between specimens included in the present study and the assignment of multiple properties would have introduced further assumptions~~ for fossil material~~.

Muscle forces and constraints. Application of jaw adductor muscle forces followed published protocols [29, 40]. Forces were based on muscle physiological cross-sectional area (PCSA) [44], corrected for pennation and gape [45], such that 1 cm^2 = 30 N[46]. Muscle forces were scaled on the basis of cranial volume to the two thirds power [40, 47] and applied using Boneload [48]. Tractions were applied to plate elements modelled as 3D membrane (thickness = 0.0001 mm; E = 20.6 GPa). We subjected all models to: a bilateral anterior tooth bite applied to the left and right incisors and canines, a unilateral anterior tooth bite at the left I^1, and a unilateral molar bite at the left M^2. Models were oriented and constrained following previous methods [40].

Automated collection of FEA results. Comparison of the VM micro-strain at 203 landmarks for each of the models in this study results in an expected 3,045 individual landmark cases. To automate the process, a function was developed ~~in Matlab to access Strand7 (v2.4) results via the application~~

~~programming interface (API) allowing for the~~to ~~-~~rapidly extract~~ion of~~ micro-strain results~~ for any number of landmarks. ~~.

Computational Fluid Dynamics.

~~[24]. Our reconstructions of the Neanderthal nasal passage alone were based on warps using 103 landmarks. ~~We used La Chapelle-aux-Saints 1 because it had the most complete nasal passage among Neanderthals. Assumptions remain of course and accuracy will ultimately be tested by the discovery of complete Neanderthal crania. However, our reconstruction and CFD clearly shows that the internal morphology of the Neanderthal nasal passage is very different to that of any of the modern humans modelled (including ULCA210, the warp source), or Broken Hill 1 (figure 3).

Estimated energy savings were calculated for a single breath in each species. We also calculated maximal airflow through the nasal passages prior to the onset of extensive turbulence through the nasal passage (and see ESM). For the three modern humans, body masses were obtained directly for UNC002 and UNC013 [36] and predicted for ULCA210 [49]. For the two extinct *Homo* body masses were obtained from previous estimates [20]. Using DICOM data and the 3D analytical program, Avizo, we generated digital casts of the left nasal passage in each of the three modern humans. The soft-tissue airway of UNC013 was used as a template for soft-tissue nasal passage shape in La Chapelle-aux-Saints 1 and Broken Hill 1, as well as ULAC210 (see ESM for further detail on soft-tissue reconstruction which follows previous methods [24]). Fluid dynamic analysis was run using Fluent (ANSYS Inc, PA).

Heat and moisture transfer were simulated for the CNP (figure S7), as the fleshy nasal vestibule is not preserved in either extinct hominin species. We used a mixed-species model to simulate water vapour transport and account for relative humidity within the nasal passage and surrounding air following previously established protocols [50]. Models were run under the widely accepted flow rate of 100 ml/s for one side of the nasal passage [51, 52] (Table S4). A second, mass-dependent flow rate was also tested (Table S5). We simulated 0°C air at 20% relative humidity. Nasal mucosa of the CNP was 37°C and assigned 100% relative humidity. CFD results are given in figure 5 and see ESM.

3. Results and discussion

FEA

We solved three load cases, comparing von Mises (VM) micro-strain generated in a: 1) bilateral anterior bite restrained at all upper incisors and canines [4], 2) a unilateral anterior bite restrained at the left upper first incisor [9], and, 3) a unilateral bite restrained at the left upper second molar for each of our 15 finite element models (FEMs) (figure 2, ESM figures 3 & 4). Muscle forces (ESM Table S1) were scaled to cranial volume following a 2/3 power rule [29, 40]. VM micro-strain was analysed from 203 homologous craniofacial landmarks grouped into 24 curves and 16 surfaces (ESM figures S3 & S4). Bite reaction forces, mechanical advantage and reaction forces at the temporomandibular joints were also computed (ESM Table S1).

From FEA of both bilateral and unilateral anterior biting Broken Hill 1 (*H. heidelbergensis*) exhibited the least mean micro-strain for all facial landmark groups (ESM figures S3 & S7). Statistical comparisons between the mean recent modern *H. sapiens* and mean *H. neanderthalensis* (ESM figure S3) revealed few significant differences. Where differences were found, the mean Neanderthal typically showed lower micro-strain than the mean recent modern human, however, in most instances one or more recent modern humans fell within the Neanderthal range (figure S7). The late Pleistocene modern human, Mladeč 1, fell within or below the Neanderthal range in almost all instances (ESM figures S3 & S7).

In unilateral anterior biting mechanical advantage was consistently higher in modern humans (mean = 0.37) than in any of the Neanderthals (mean = 0.32), which in turn recorded slightly higher mechanical advantage than *H. heidelbergensis* (0.29). This is reflected in the bite reaction forces (BRF) at the anterior teeth in loadings where muscle forces were scaled to the volume$^{2/3}$ of bone in the cranium. In *Homo heidelbergensis* (Broken Hill 1), which exhibited the highest cranial volume and muscle forces, BRF was 428 Newtons (N), above either the mean (371 N) or any individual result for the three Neanderthals. However, the distinction was less clear compared to the modern human sample, which, despite much lower muscle forces (70% that of Broken Hill 1) recorded a mean of 399 N.

Our predictions of mechanical performance during a unilateral bite at M^2 revealed even fewer significant differences in micro-strain between the mean recent modern human and mean Neanderthal (ESM figure S4). Mechanical advantage in molar biting is slightly lower for Broken Hill 1 (0.48) than for the mean Neanderthal (0.50), although within the Neanderthal range (ESM Table S1). For all modern humans mechanical advantage (mean = 0.67) is well above that of either Broken Hill 1 or any of the Neanderthals (Table 1). Again this is reflected in the M^2 bite reaction force data. BRF at M^2 for Broken Hill 1 (719 N) was above either the mean or any individual BRF at M^2 for the three Neanderthals (Mean = 581 N). While, despite much lower muscle forces, mean BRF at M^2 for modern humans (719 N) was identical to that computed for Broken Hill 1 and four of the modern humans generated higher BRFs at M^2 than did Broken Hill 1 (ESM Table S1).

Considered together with the VM micro-strain results, we find no clear support for the argument that the facial morphology of Neanderthals is an adaptation linked to heavy anterior biting. Although we found that Neanderthals have higher average mechanical advantage in biting at the anterior teeth than Broken Hill 1, differences were minor and micro-strain was relatively high in the Neanderthals, despite higher bite reaction forces in *H. heidelbergensis*. In unilateral biting at M^2 *H. heidelbergensis* fell within the Neanderthal range for mechanical advantage, but again generated higher bite reaction forces while exhibiting less micro-strain.

TMJ reaction forces were uniformly in tension in unilateral M^2 biting for the modern humans, suggesting that they cannot exert maximal muscle forces concurrently on working and balancing sides in biting at M^2 without generating distractive forces on the working side [53, 54]. The functional significance of this remains uncertain because a relatively modest reduction in muscle force on the balancing side brings the working side back into compression, with only slight reduction to bite reaction force [54]. Working-to-balancing-side asymmetry in muscle recruitment is commonly observed in primates [55].

There is a~~n interesting~~ potential trade-off in unilateral molar biting, in that increased mechanical efficiency allows a more powerful bite reaction force for any given muscle force, and, a reduced need for heavy supporting structures for any given BRF [26], but beyond the point at which the balancing side TMJ goes into tension some reduction in muscle recruitment and hence reduction in bite reaction force is required. The real cost of this increased mechanical efficiency in modern humans might be a loss of available molar occlusal area rather than reduced bite force. The potential benefit is a reduction in the musculature, bone and energy required.

CFD

It is important to note that the modern European (ULCA210) used to generate the source CFD mesh in our Neanderthal reconstruction, behaved in all respects most like the other ethnic European (UNC002) and was very distinct from either the Neanderthal or Broken Hill 1 (see figure 35).

All three species effectively conditioned inspired air. However, modern humans were the most efficient, recovering 84–96% of energy used. The La Chapelle-aux-Saints 1 nasal passage was 8-10% less effective than those of the modern humans, and Broken Hill 1 was the least efficient (5–15% and 9.5–25% less efficient than La Chapelle-aux-Saints 1 and the modern humans respectively) (figure 3 and Tables S3–S4). Our CFD results are not necessarily inconsistent with recently published data for a Neanderthal and two modern humans [25], but cannot be directly compared because of differences in material and approach. Notably the previous results were based analyses which only considered the external morphology of the nasal passage. The ensuing model based on 11 landmarks did not address internal nasal passage geometry. Our Neanderthal model nasal passage was based on a 'warp' which included 103 landmarks, 54 of which were internal landmarks. Previous studies have shown that using a higher number of landmarks across warped source models will produce more accurate target models [39, 56].

At 18,723 mm^3, the reconstructed Neanderthal nasal passage was ~29% larger than the average volume of the modern humans (14,487 mm^3), which were in turn considerably greater than that of Broken Hill 1 (11,751 mm^3). However, total volume of the nasal passage is not the sole predictor of maximal airflow rates, which are also influenced by the interaction of lung tidal volume, breathing frequency, and the calibre of the conducting portion of the respiratory system. In humans, the size of the nostril and nasal valve are the strongest determinants of flow rate limits. Although smaller calibre air spaces are found deeper in the nasal passage (e.g., the olfactory slit / superior meatus), their effect on flow rate can be offset by larger calibre openings located within the same cross sectional plane, allowing more air to pass by without requiring excessive air speeds to maintain continuity. In contrast, all inspired air must pass through the nostril and choana, making these the prime choke points for airflow within the nasal passage. As the nostril is the smaller of the two openings, it will impose a greater limit on airflow. Based on predicted nostril sizes for La Chapelle-aux-Saints 1 and Broken Hill 1 (see ESM), our CFD analyses predicted that the Neanderthal could move almost twice the volume of air through their nasal passages under laminar conditions than modern humans (~50 Litres/minute (L/m) in Neanderthal vs

~27 L/m in modern humans). Despite its lower total nasal volume, predicted nostril size in Broken Hill 1 (see ESM) gave a maximum airflow rate of ~42 L/m, lower than for the Neanderthal, but still substantially higher than in the modern humans.

Our results indicate that nasal passage shape, rather than total nasal cavity size, is the critical factor here (and see ESM). Results are in agreement with the proposition that Neanderthals, and to a lesser extent, Broken Hill 1, may have had considerably higher energetic demands than modern humans, a finding consistent with predictions of both Neanderthal and *H. heidelbergensis* physiology [20, 21, 57] and lung volume [58]. A further point to consider is that this capacity to move more air through the nasal cavity would have conferred a higher nasal to oral breathing threshold on Neanderthals, allowing them to benefit from the air conditioning and pathogen/pollutant filtering capacity [59] of the nose over a wider range of flow rates than other human species.

4. Conclusions.

Our results show that, compared to either the likely more 'primitive' condition in *H. heidelbergensis*, or the independently derived condition in modern humans, Neanderthals are not clearly better-adapted to sustain high loads on the anterior teeth and Hypothesis 1 is rejected. However, relative to the likely pleisiomorphic condition, Neanderthal nasal passage morphology may represent an adaptation to cold that improves conditioning of inspired air, albeit a less efficient solution to that found in modern humans. These findings are consistent with Hypothesis 2. Our results further suggest that the Neanderthal capacity to move greater air volumes than either Broken Hill 1, or modern humans, may also represent an adaptation to cold, insofar as it could support a cold climate physiology [57]. An alternative, not mutually exclusive explanation, is that this ability reflects an adaptation to a more strenuous, energetically demanding lifestyle demanding high calorific intakes. It has been calculated that Neanderthals used 3,360 to 4,480 kcal per day to support winter foraging and cold resistance [21]. Consequently we conclude that Hypothesis 3 is also supported and that the distinctive facial morphology of Neanderthals has been driven, at least in part, by adaptation to cold, both regarding the conditioning of inspired air and a greater ventilatory capacity demanded by cold resistance.

Ethics. Research conducted for this study was largely performed on skeletal and fossil specimens that are reposited in accredited museums. The protocols for collection and use of scans for UNC013 and UNC002 were reviewed and approved by the Duke University and University of North Carolina Institutional Review Boards. IRB numbers are DUMC IRB 4881-03 and UNC-CH IRB 03-Surg-372.

Data accessibility. All data, code and results needed to replicate this study are available from Dryad [doi:10.5061/dryad.39272]. Additional results and supplemental methods have been uploaded as part of the electronic supplementary material (ESM). CT scan data is reposited with the museums/institutes that hold copyright; requests to use scan data should be made directly to those museums/institutes.

Author Contributions. S.W. & W.C.H.P. conceived and developed experimental design. W.C.H.P. generated 'warps' for virtual reconstructions. W.C.H.P., J.L., J.B. & S.W. conducted analyses. S.W., W.C.H.P., J.L., J.B., S.P.E., L.F., S.B., J.J.H., C.S., O.K., M.C., T.C.R. & T.K. contributed data. S.W. wrote the MS with contributions from all other authors. To whom correspondence should be addressed. E-mail: S.W. (swroe@une.edu.au) or W.C.H.P. (w.parr@unsw.edu.au).

Funding. Research was supported by an Australian Research Council Discovery Grant DP140102659 to S.W., W.C.H.P., & L.F.

Acknowledgements. We thank Almut Hoffmann (Museum für Vor und Frühgeschichte, Berlin) and Andreas Winzer (Department of Human Evolution, MPI) for access to fossil material, and three anonymous reviewers as well as editorial staff for feedback.

References

[1] Trinkaus, E. 1987 The Neandertal face: evolutionary and functional perspectives on a recent hominid face. *J. Human Evol.* **16**, 429-443.
[2] Franciscus, R.G. 1999 Neandertal nasal structures and upper respiratory tract "specialization.". *Proc. Natl. Acad. Sci. USA* **96**, 1805-1809.
[3] Trinkaus, E. 2003 Neandertal faces were not long; modern human faces are short. *Proc. Natl. Acad. Sci. U.S.A.* **100**, 8142-8145. (doi:10.1073/pnas.1433023100).
[4] Rak, Y. 1986 The Neanderthal: a new look at an old face. *J. Human Evol.* **15**, 151-164.
[5] Coon, C.S. 1962 *The origin of races*. New York, Knopf.
[6] Weaver, T.D. 2009 The meaning of Neandertal skeletal morphology. *Proc. Natl. Acad. Sci. U.S.A.* **106**, 16028-16033. (doi:10.1073/pnas.0903864106).
[7] Clement, A.F., Hillson, S.W. & Aiello, L.C. 2012 Tooth wear, Neanderthal facial morphology and the anterior dental loading hypothesis. *J. Human Evol.* **62**, 367-376. (doi:http://dx.doi.org/10.1016/j.jhevol.2011.11.014).

[8] Demes, B. 1987 Another look at an old face: biomechanics of the neandertal facial skeleton reconsidered. *J. Human Evol.* **16**, 297-303.
[9] Spencer, M.A. & Demes, B. 1993 Biomechanical analysis of masticatory system configuration in Neandertals and Inuits. *Am. J. Phys. Anthropol.* **91**, 1-20. (doi:10.1002/ajpa.1330910102).
[10] O'Connor, C.F., Franciscus, R.G. & Holton, N.E. 2005 Bite force production capability and efficiency in neanderthals and modern humans. *Am. J. Phys. Anthropol.* **127**, 129-151.
[11] Maddux, S.D., Butaric, L.N., Yokley, T.R. & Franciscus, R.G. 2017 Ecogeographic variation across morphofunctional units of the human nose. *Am. J. Phys. Anthropol.* **162**, 103-119. (doi:10.1002/ajpa.23100).
[12] Maddux, S.D., Yokley, T.R., Svoma, B.M. & Franciscus, R.G. 2016 Absolute humidity and the human nose: A reanalysis of climate zones and their influence on nasal form and function. *Am. J. Phys. Anthropol.* **161**, 309-320. (doi:10.1002/ajpa.23032).
[13] Churchill, S. 1998 Cold adaptation, heterochrony, and neanderthals. *Evol. Anthr.* **7**, 46-61.
[14] Rae, T., Koppe, T. & Stringer, C.B. 2011 The Neanderthal face is not cold-adapted. *J. Human Evol.* **60**, 234-239.
[15] Holton, N.E., Yokley, T.R. & Franciscus, R.G. 2011 Climatic adaptation and Neandertal facial evolution: A comment on Rae et al. (2011). *J. Human Evol.* **61**, 624-627. (doi:http://dx.doi.org/10.1016/j.jhevol.2011.08.001).
[16] Holton, N., Yokley, T. & Butaric, L. 2013 The Morphological Interaction Between the Nasal Cavity and Maxillary Sinuses in Living Humans. *Anat. Rec.* **296**, 414-426. (doi:10.1002/ar.22655).
[17] Bastir, M. & Rosas, A. 2013 Cranial airways and the integration between the inner and outer facial skeleton in humans. *Am. J. Phys. Anthropol.* **152**, 287-293. (doi:10.1002/ajpa.22359).
[18] Jelinek, A.J. 1994 Hominids, Energy, Environment, and Behavior in the Late Pleistocene. In *Origins of Anatomically Modern Humans* (eds. M.H. Nitecki & D.V. Nitecki), pp. 67-92. Boston, MA, Springer US.
[19] Churchill, S.E. 2014 Surviving the Cold. In *Thin on the Ground* (pp. 107-150, John Wiley & Sons, Inc.
[20] Froehle A.W., Y.T.R., Churchill S. E. 2013 Energetics and the origin of modern humans. In *The Origins of Modern Humans: Biology Reconsidered* (ed. A.J.C.M. Smith F. H.), pp. 285-320. Hoboken, Wiley-Blackwell.
[21] Steegmann, A.T., Cerny, F.J. & Holliday, T.W. 2002 Neandertal cold adaptation: Physiological and energetic factors. *Am. J. Hum. Biol.* **14**, 566-583. (doi:10.1002/ajhb.10070).
[22] Berger, T.D. & Trinkaus, E. 1995 Patterns of Trauma among the Neandertals. *Journal of Archaeological Science* **22**, 841-852. (doi:https://doi.org/10.1016/0305-4403(95)90013-6).
[23] Nishimura, T., Mori, F., Hanida, S., Kumahata, K., Ishikawa, S., Samarat, K., Miyabe-Nishiwaki, T., Hayashi, M., Tomonaga, M., Suzuki, J., et al. 2016 Impaired Air Conditioning within the Nasal Cavity in Flat-Faced *Homo*. *PLoS Comput. Biol.* **12**, e1004807. (doi:10.1371/journal.pcbi.1004807).
[24] Bourke, J.M., Ruger Porter, W.M., Ridgely, R.C., Lyson, T.R., Schachner, E.R., Bell, P.R. & Witmer, L.M. 2014 Breathing Life Into Dinosaurs: Tackling Challenges of Soft-Tissue Restoration and Nasal Airflow in Extinct Species. *Anat. Rec.* **297**, 2148-2186. (doi:10.1002/ar.23046).
[25] de Azevedo, S., González, M.F., Cintas, C., Ramallo, V., Quinto-Sánchez, M., Márquez, F., Hünemeier, T., Paschetta, C., Ruderman, A., Navarro, P., et al. 2017 Nasal airflow simulations suggest convergent adaptation in Neanderthals and modern humans. *Proceedings of the National Academy of Sciences*. (doi:10.1073/pnas.1703790114).
[26] Wroe, S., Ferrara, T.L., McHenry, C.R., Curnoe, D. & Chamoli, U. 2010 The craniomandibular mechanics of being human. *Proc. R. Soc. Lond. [Biol.]* **277**, 3579-3586.
[27] Rayfield, E.J. 2007 Finite Element Analysis and Understanding the Biomechanics and Evolution of Living and Fossil Organisms. *Annu. Rev. Earth Planet. Sci.* **35**, 541-576.
[28] Dumont, E.R., Piccirillo, J. & Grosse, I.R. 2005 Finite-element analysis of biting behavior and bone stress in the facial skeletons of bats. *The Anatomical Record Part A* **283A**, 319-330.
[29] Ledogar, J.A., Smith, A.L., Benazzi, S., Weber, G.W., Spencer, M.A., Carlson, K.B., McNulty, K.P., Dechow, P.C., Grosse, I.R., Ross, C.F., et al. 2016 Mechanical evidence that *Australopithecus sediba* was limited in its ability to eat hard foods. *Nat. Commun.* **7**. (doi:10.1038/ncomms10596).
[30] Strait, D.S., Weber, G.W., Neubauer, S., Chalk, J., Richmond, B.G., Lucas, P.W., Spencer, M.A., Schrein, C., Dechow, P.C., Ross, C.F., et al. 2009 The feeding biomechanics and dietary ecology of *Australopithecus africanus*. *Proc. Natl. Acad. Sci. U.S.A.* **106**, 2124-2129.
[31] Wroe, S., Moreno, K., Clausen, P., McHenry, C. & Curnoe, D. 2007 High resolution three-dimensional computer simulation of hominid cranial mechanics. *Anat. Rec.* **290**, 1248-1255.

[32] Ledogar, J.A., Benazzi, S., Smith, A.L., Weber, G.W., Carlson, K.B., Dechow, P.C., Grosse, I.R., Ross, C.F., Richmond, B.G., Wright, B.W., et al. 2017 The Biomechanics of Bony Facial “Buttresses” in South African Australopiths: An Experimental Study Using Finite Element Analysis. *Anat. Rec.* **300**, 171-195. (doi:10.1002/ar.23492).

[33] Parr, W., Wroe, S., Chamoli, U., Richards, H.S., McCurry, M., Clause, P.D. & McHenry, C.R. 2012 Toward integration of geometric morphometrics and computational biomechanics: New methods for 3D virtual reconstruction and quantitative analysis of Finite Element Models. *Journal of Theoretical Biology* **301**, 1-14.

[34] O'Higgins, P., Cobb, S.N., Fitton, L.C., Groning, F., Phillips, R., Liu, J. & Fagan, M.J. 2011 Combining geometric morphometrics and functional simulation: an emerging toolkit for virtual functional analyses. *J. Anat.* **218**, 3-15.

[35] Smith, A.L., Benazzi, S., Ledogar, J.A., Tamvada, K., Smith, L.C.P., Weber, G.W., Spencer, M.A., Dechow, P.C., Grosse, I.R., Ross, C.F., et al. 2015 Biomechanical implications of intraspecific shape variation in chimpanzee crania: moving towards an integration of geometric morphometrics and finite element analysis. *Anatomical record (Hoboken, N.J. : 2007)* **298**, 122-144. (doi:10.1002/ar.23074).

[36] Yokley, T.R. 2009 Ecogeographic variation in human nasal passages. *Am. J. Phys. Anthropol.* **138**, 11-22. (doi:10.1002/ajpa.20893).

[37] Mounier, A. & Mirazón Lahr, M. 2016 Virtual ancestor reconstruction: Revealing the ancestor of modern humans and Neandertals. *J. Human Evol.* **91**, 57-72. (doi:https://doi.org/10.1016/j.jhevol.2015.11.002).

[38] Senck, S., Coquerelle, M., Weber, G.W. & Benazzi, S. 2013 Virtual Reconstruction of Very Large Skull Defects Featuring Partly and Completely Missing Midsagittal Planes. *Anat. Rec.* **296**, 745–758. (doi:10.1002/ar.22693).

[39] Gunz, P., Mitteroecker, P., Neubauer, S., Weber, G.W. & Bookstein, F.L. 2009 Principles for the virtual reconstruction of hominin crania. *J. Human Evol.* **57**, 48-62.

[40] Ledogar, J.A., Dechow, P.C., Wang, Q., Gharpure, P.H., Gordon, A.D., Baab, K.L., Smith, A.L., Weber, G.W., Grosse, I.R., Ross, C.F., et al. 2016 Human feeding biomechanics: performance, variation, and functional constraints. *PeerJ* **4**, e2242. (doi:10.7717/peerj.2242).

[41] McHenry, C.R., Wroe, S., Clausen, P.D., Moreno, K. & Cunningham, E. 2007 Supermodeled sabercat, predatory behavior in *Smilodon fatalis* revealed by high-resolution 3D computer simulation. *Proc. Natl. Acad. Sci. U.S.A.* **104**, 16010-16015.

[42] Strait, D.S., Wang, Q., Dechow, P.C., Ross, C.F., Richmond, B.G., Spencer, M.A. & Patel, B.A. 2005 Modeling elastic properties in finite-element analysis: How much precision Is needed to produce an accurate model? *Anat. Rec.* **283A**, 275-287.

[43] Chamoli, U. & Wroe, S. 2011 Allometry in the distribution of material properties and geometry of the felid skull: Why larger species may need to change and how they may achieve it. *Journal of Theoretical Biology* **283**, 217-226. (doi:10.1016/j.jtbi.2011.05.020).

[44] van Eijden, T.M.G.J., Korfage, J.A.M. & Brugman, P. 1997 Architecture of the human jaw-closing and jaw-opening muscles. *Anat. Rec.* **248**, 464-474. (doi:10.1002/(SICI)1097-0185(199707)248:3<464::AID-AR20>3.0.CO;2-M).

[45] Taylor, A.B. & Vinyard, C.J. 2013 The relationships among jaw-muscle fiber architecture, jaw morphology, and feeding behavior in extant apes and modern humans. *Am. J. Phys. Anthropol.* **151**, 120-134. (doi:10.1002/ajpa.22260).

[46] Murphy, R.A. 1998 Skeletal muscle. In *Physiology* (eds. R.M. Berne & M.N. Levy), p. 294. St Loius, Mosby.

[47] Strait, D.S., Grosse, I.R., Dechow, P.C., Smith, A.L., Wang, Q., Weber, G.W., Neubauer, S., Slice, D.E., Chalk, J., Richmond, B.G., et al. 2010 The Structural Rigidity of the Cranium of *Australopithecus africanus*: Implications for Diet, Dietary Adaptations, and the Allometry of Feeding Biomechanics. *The Anatomical Record: Advances in Integrative Anatomy and Evolutionary Biology* **293**, 583-593.

[48] Grosse, I.R., Dumont, E.R., Coletta, C. & Tolleson, A. 2007 Techniques for modeling muscle-Induced forces in finite element models of skeletal structures. *Anat. Rec.* **290**, 1069-1088.

[49] Kappelman, J. 1996 The evolution of body mass and relative brain size in fossil hominids. *J. Human Evol.* **30**, 243-276. (doi:https://doi.org/10.1006/jhev.1996.0021).

[50] Naftali, S., Rosenfeld, M., Wolf, M. & Elad, D. 2005 The air-conditioning capacity of the human nose. *Ann Biomed Eng* **33**. (doi:10.1007/s10439-005-2513-4).

[51] Doorly, D.J., Taylor, D.J., Gambaruto, A.M., Schroter, R.C. & Tolley, N. 2008 Nasal architecture: form and flow. *Philos. Trans. Roy. Soc. London Ser. A* **366**, 3225-3246. (doi:10.1098/rsta.2008.0083).

[52] Weinhold, I. 2004 Numerical Simulation of Airflow in the Human Nose. *Eur. Arch. Otorhinolaryngol.* **261**, 452-455.
[53] Greaves, W.S. 1978 The jaw lever system in ungulates: a new model. *J Zool Lond* **184**, 271–285.
[54] Clausen, P., Wroe, S., McHenry, C., Moreno, K. & Bourke, J. 2008 The vector of jaw muscle force as determined by computer-generated three dimensional simulation: A test of Greaves' model. *J. Biomech.* **41**, 3184-3188.
[55] Hylander, W.L., Ravosa, M.J., Ross, C.F. 2004 Jaw muscle recruitment patterns during mastication in anthropoids and prosimians. In *Shaping primate evolution* (ed. F. Anapol, German, R.Z., Jablonski N.J.), pp. 229–257. Cambridge, Cambridge University Press.
[56] Parr, W.C.H., Wroe, S., Chamoli, U., Richards, H.S., McCurry, M.R., Clausen, P.D. & McHenry, C. 2012 Toward integration of geometric morphometrics and computational biomechanics: New methods for 3D virtual reconstruction and quantitative analysis of Finite Element Models. *Journal of Theoretical Biology* **301**, 1-14. (doi:http://dx.doi.org/10.1016/j.jtbi.2012.01.030).
[57] Fiorenza, L., Benazzi, S., Henry, A., Salazar-García, D.C., Blasco, R., Picin, A., Wroe, S. & Kullmer, O. 2015 To meat or not to meat? New perspectives on Neanderthal ecology. *Am. J. Phys. Anthropol.* **156**, (S59) 43-71.
[58] Weinstein, K.J. 2008 Thoracic morphology in Near Eastern Neandertals and early modern humans compared with recent modern humans from high and low altitudes. *J. Human Evol.* **54**, 287-295. (doi:http://dx.doi.org/10.1016/j.jhevol.2007.08.010).
[59] White, D.E., Bartley, J. & Nates, R.J. 2015 Model demonstrates functional purpose of the nasal cycle. *Biomed. Eng. Online* **14**, 1-11. (doi:10.1186/s12938-015-0034-4).

Figure captions

Figure 1. La Chapelle-aux-Saints 1 Neanderthal mesh-mesh metric comparison of initial fossil material (A) with final reconstruction (B) (performed in Cloud Compare). The models are superimposed (C) and the original-reconstructed mesh-mesh metrics are computed. Regions where the final reconstruction lies further out (from the model centroid) than the original fossil material are shown in blue. Regions where the final reconstruction lies further in (from the model centroid) than the original fossil material are shown in red. Regions of the original fossil material that lie further than +/- 1.875 mm (3 voxel edge lengths) from the final reconstruction have been clipped from the image. Regions that overlap almost exactly are shown in off-white.

Figure 2. Results of Finite Element Analysis under an anterior bite simulation (loading via muscle force scaled to volume$^{2/3}$, restraints applied to incisors and canines) for ten recent (A-J) and one Pleistocene (K) modern human, as well as *H. heidelbergensis* (L), and three *H. neanderthalensis* (M-O). Number of elements for each models also given for: A) Khoe-San female, 1,571,213, B) Caucasian male, 1,602,686, C) European female, 1,651,738, D) Chinese male, 1,593,342, E) Malay female, 1,608,934, F) Inuit male, 1,625,463, G) Inuit female, 1,700,708, H) Pacific Islander male, 1,701,642, I) Peruvian female, 1,619,268, J) European male, 1,651,945, K) Mladeč 1, 1,724,664, L) Broken Hill 1, 1,611,994, M) La Ferrassie 1, 1,618,373, N) La Chapelle-aux-Saints 1, 1,625,022, and O) Gibraltar 1, 1,609,723.

Figure 3. Figure 5. Heat flow through the left nasal passage of a (A) *Homo heidelbergensis*, (B) *Homo neanderthalensis*, and (C) *Homo sapiens* (UNC002). (D) *Homo sapiens* (ULAC210). (E) *Homo sapiens* (UNC013). Heat transfer is shown in cross sections taken at numbered regions in each nasal passage, and shown under both 100 ml/s and the mass-dependent flow rate.

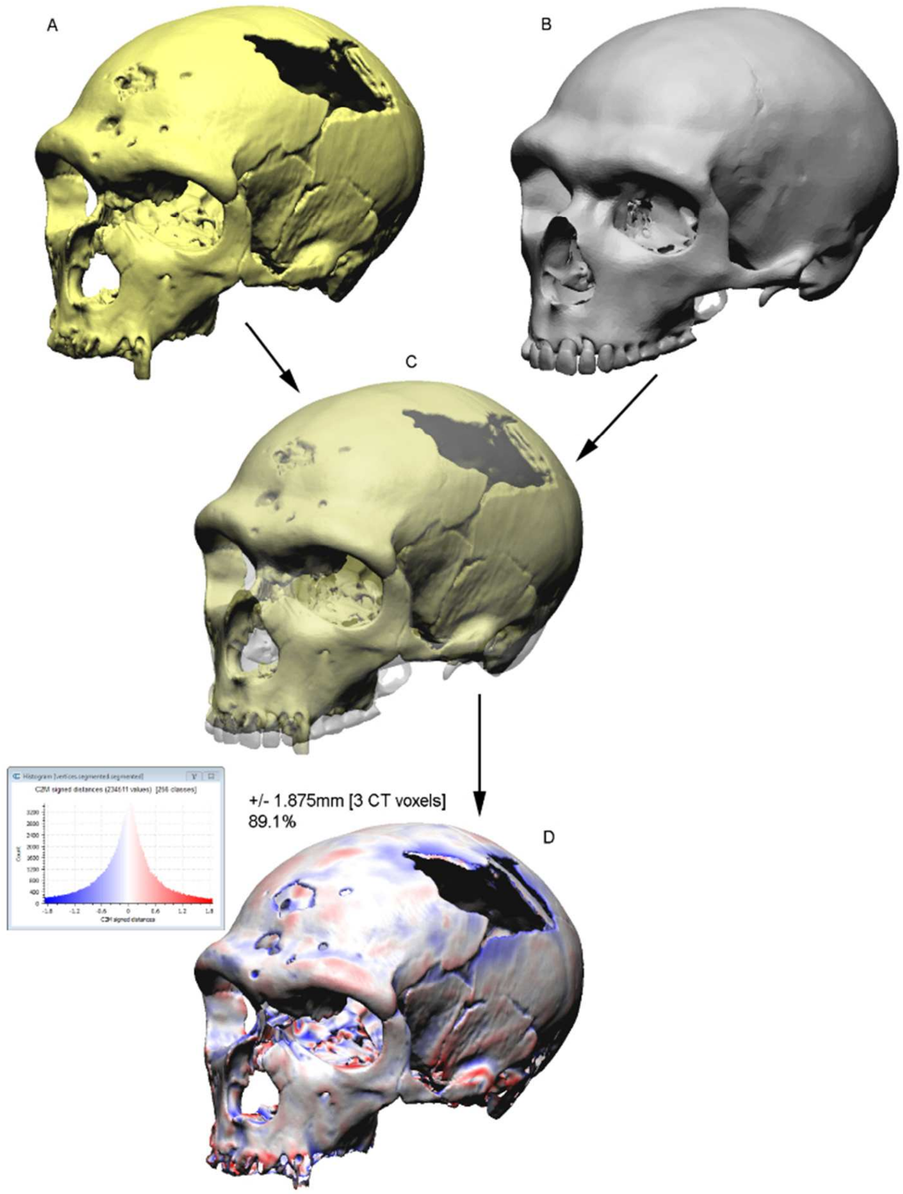

87x116mm (220 x 220 DPI)

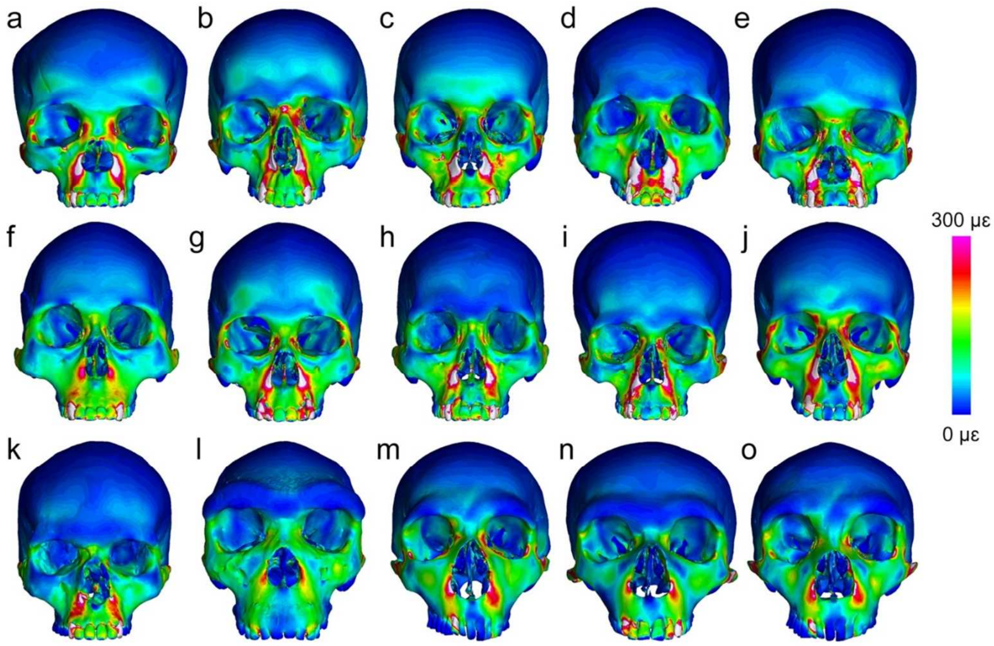

156x102mm (220 x 220 DPI)

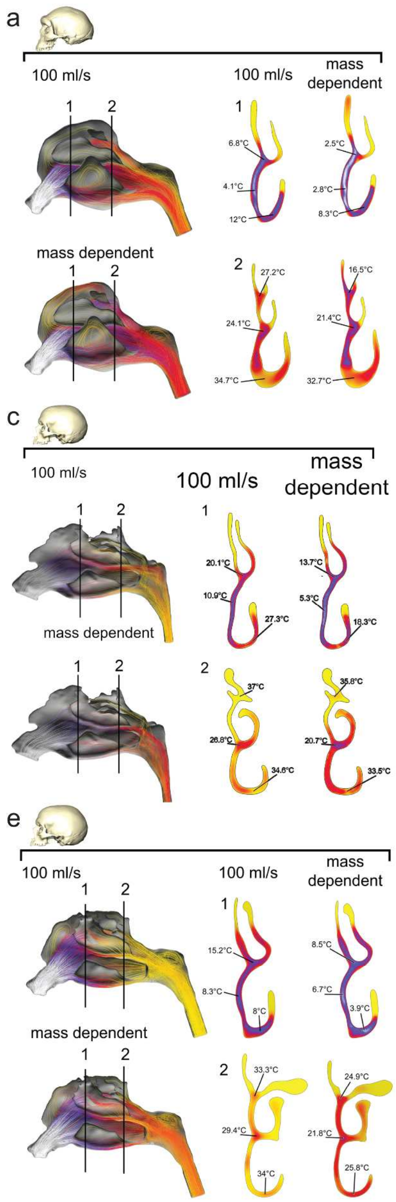

207x295mm (300 x 300 DPI)